COGNITIVE NEUROSCIENCE

Noninvasive modulation of the hippocampal-entorhinal complex during spatial navigation in humans

Elena Beanato[1,2]†, Hyuk-June Moon[3,4]†, Fabienne Windel[1,2]‡, Pierre Vassiliadis[1,2]‡, Maximillian J. Wessel[1,2,5]‡, Traian Popa[1,2,6], Menoud Pauline[1,2], Esra Neufeld[7,8], Emanuela De Falco[3], Baptiste Gauthier[3], Melanie Steiner[7], Olaf Blanke[3,9]*§, Friedhelm C. Hummel[1,2,9]*§

Because of the depth of the hippocampal-entorhinal complex (HC-EC) in the brain, understanding of its role in spatial navigation via neuromodulation was limited in humans. Here, we aimed to better elucidate this relationship in healthy volunteers, using transcranial temporal interference electric stimulation (tTIS), a noninvasive technique allowing to selectively neuromodulate deep brain structures. We applied tTIS to the right HC-EC in either continuous or intermittent theta-burst stimulation patterns (cTBS or iTBS), compared to a control condition, during a virtual reality–based spatial navigation task and concomitant functional magnetic resonance imaging. iTBS improved spatial navigation performance, correlated with hippocampal activity modulation, and decreased grid cell–like activity in EC. Collectively, these data provide the evidence that human HC-EC activity can be directly and noninvasively modulated leading to changes of spatial navigation behavior. These findings suggest promising perspectives for patients suffering from cognitive impairment such as following traumatic brain injury or dementia.

INTRODUCTION

Cognitive deficits in navigation and spatial memory are commonly observed in the aging population (*1*–*3*) and in neurodegenerative conditions ranging from mild cognitive impairment to dementia, including Alzheimer's disease (*4*, *5*). Deterioration of these functions highly influences daily life and the autonomy of the affected individuals (*6*), and, thus, many efforts have been made to better understand the brain networks underlying them (*7*–*9*) as a starting point for the development of innovative treatment strategies. Decades of research in animals and humans have demonstrated that spatial navigation and memory functions depend on regions of the medial temporal lobe (MTL), including the hippocampus and entorhinal cortex (*10*–*12*). The hippocampal-entorhinal complex (HC-EC) in the MTL has been highlighted as a core region for spatial cognitive functions, including the discovery of the well-studied place and grid cells (*10*, *13*–*18*). These cells were identified on the basis of their spatial-selective firings (i.e., they fire at specific subject locations in space). In particular, grid cells manifest characteristic geometrically arranged firing patterns, composing a hexagonal grid (*14*). Together with other types of specialized cells, place and grid cells are thought to create a mental map of the environment that supports spatial navigation and memory (*15*). While these findings have been well established in animal studies, translation to humans has been challenging because of the invasiveness of grid cell recordings (*19*), limiting the possibility to assess their causal impacts on behavior (*20*, *21*). However, in a seminal study, Doeller *et al.* (*22*) observed grid cell–like representation (GCLR) in humans in a noninvasive, associative way, via functional magnetic resonance imaging (fMRI), which is thought to reflect the activation of grid cells in EC. GCLR is an fMRI signal change that exhibits a sixfold symmetry according to heading direction. fMRI signals are expected to be higher when a participant moves in a direction aligned with the hexagonal grid than in a misaligned direction. Since a hexagonal grid has six axes, the signal changes will demonstrate a sixfold symmetry. This measure has been replicated and refined subsequently by several other research groups (*23*–*25*). An interesting relationship between the hippocampus and entorhinal grid cell–like activity has also been found, identifying hippocampal activity as a compensatory mechanism in case of GCLR alteration (*23*). Nonetheless, further investigations are needed to understand (i) the causal role of the HC-EC complex and grid cell–like activity in human spatial cognitive functions, (ii) the impact of age and neurological diseases on it, and (iii) on the basis of what is learned, how to reinstate healthy functioning.

Noninvasive brain stimulation (NIBS) is a well-established approach to modulate neural activity and probe causal relationships between a targeted region and associated brain activity or behavior (*26*). Therefore, it would be desirable to apply NIBS to test in humans the hypothesized causal involvement of the HC-EC and GCLR in spatial cognitive functions. However, conventional NIBS methods, including transcranial electrical stimulation and transcranial magnetic stimulation (TMS) are not able to reach deep structures like the MTL in a focal way due to their steep depth-focality tradeoff (*27*). An increase in stimulation intensity, to reach deeper target regions, will unequivocally lead to substantial concomitant stimulation of overlying cortical areas (*28*). Because of this limitation, studies investigating possible modulation of MTL functions were until

[1]Defitech Chair of Clinical Neuroengineering, Neuro-X Institute (INX), École Polytechnique Fédérale de Lausanne (EPFL), Geneva, Switzerland. [2]Defitech Chair of Clinical Neuroengineering, Neuro-X Institute (INX), Clinique Romande de Réadaptation, École Polytechnique Fédérale de Lausanne (EPFL Valais), Sion, Switzerland. [3]Laboratory of Cognitive Neuroscience, Neuro-X Institute (INX), École Polytechnique Fédérale de Lausanne (EPFL), Geneva, Switzerland. [4]Center for Bionics, Biomedical Research Institute, Korea Institute of Science and Technology (KIST), Seoul, South Korea. [5]Department of Neurology, University Hospital Würzburg, Würzburg, Germany. [6]Department of Clinical Neurosciences, Lausanne University Hospital and University of Lausanne, Lausanne, Switzerland. [7]Foundation for Research on Information Technologies in Society (IT'IS), Zurich, Switzerland. [8]ZMT Zurich MedTech AG, Zurich, Switzerland. [9]Department of Clinical Neuroscience, University of Geneva Medical School, Geneva, Switzerland.
*Corresponding author. Email: friedhelm.hummel@epfl.ch (F.C.H); olaf.blanke@epfl.ch (O.B.)
†These authors contributed equally to this work.
‡These authors contributed equally to this work.
§These authors contributed equally to this work.

now limited to invasive methods (*29*–*31*), i.e., deep brain stimulation (DBS) in already implanted patients. Transcranial temporal interference electric stimulation (tTIS) is a NIBS technique recently introduced in rodents, which is able to overcome this limitation (*32*) without the risks associated with invasive approaches. tTIS uses two pairs of electrodes delivering high-frequency (HF) electrical currents, which are not effectively affecting brain activity (*32*, *33*). However, after applying a small-frequency shift between the two pairs in the firing range of neurons, the superposition of the currents results in a modulated envelope oscillating at the frequency difference able to influence neuronal activity. The modulation depth can be maximized in deep brain regions while minimizing it in the overlying tissues (*32*). Moreover, the modulation amplitude peak can not only be steered by changing electrode positions but also by adapting the relative current magnitudes of the two channels (*34*). Recent human studies support the translational potential and the feasibility to focally modulate deep structures such as the striatum (*35*, *36*) and the HC (*37*, *38*). tTIS was successfully applied to the striatum to support brain plasticity most likely via long-term potentiation (LTP)–like effects (*35*). Further validation of the technology has been recently provided by applying oscillatory tTIS to hippocampal regions during a face-name association task (*37*), with a mirrored montage with respect to the one used in the present study (to target the left hippocampal complex instead of the right one). This previous work confirms the feasibility of targeting the HC in a focal manner by both cadaver and human fMRI experiments. Results from these first studies make tTIS an extremely promising method to focally target and modulate deep brain regions noninvasively (*39*, *40*), as well as to test their impact on spatial navigation.

There is strong evidence on the role of theta oscillations within the MTL during spatial navigation functions in both animals (*13*, *41*, *42*) and human studies (*25*, *43*–*45*). Theta rhythms are observed during both encoding and retrieval periods of navigation (*44*), are associated with memory performances (*13*, *46*), and have also been linked to the grid cell–like modulation during spatial navigation (*47*). Application of stimulation bursts in the theta frequency range has been initially proposed to mimic the natural hippocampal theta rhythms and has been shown to induce LTP and long-term depression (LTD) effects in animal brain slices (*48*). On the basis of robust in vitro results, the stimulation protocol has been translated to humans by means of TMS. In this context, theta burst stimulation (TBS) has been frequently applied either in an intermittent or continuous fashion, as iTBS and cTBS, respectively (*49*–*52*). The two protocols originally showed opposite effects when targeting cortical layers using TMS, with iTBS pattern inducing LTP-like and a cTBS pattern leading to LTD-like effects (*52*). Yet, the depth-focality trade-off characterizing current NIBS techniques prevented the noninvasive investigation of iTBS and cTBS effects on subcortical structures such as the hippocampus (similar to the original slice work) in healthy humans. Because of our prior experience in successfully modulating striatal activity and increase of behavioral performance via iTBS-tTIS (*35*), we aimed at testing iTBS-tTIS as the main stimulation technique to improve spatial navigation functions. As a control stimulation, we choose cTBS-tTIS as an active control condition with potentially opposite effect, as suggested by previous TMS results (*52*).

Building on these findings, the current work aimed at investigating the possibility to noninvasively modulate HC-EC activity including GCLR, unveiling information on the causal link between HC-EC and spatial navigation/memory in humans. This was achieved by integrating fMRI and an MR-compatible immersive virtual reality (VR) system with cutting-edge noninvasive deep brain stimulation technology (tTIS). Our immersive VR setup, which was previously shown to activate the entorhinal GCLR (*53*), provided a realistic yet controlled task environment for the participants to navigate, enhancing the fidelity of our data. Moreover, the concurrent use of fMRI allowed for assessing the corresponding changes in activity in the relevant neural representations.

Here, we noninvasively targeted the right HC-EC, which has been more closely related to the spatial memory/navigation than the left side (*54*–*56*), with tTIS, while participants performed a VR-based navigation task in the MRI scanner. Two active protocols, namely iTBS and cTBS, and a tTIS control stimulation (control) were applied in a randomized, double-blind design.

RESULTS

iTBS was associated with faster departure time

The participants performed six blocks of a VR spatial navigation task (please see Fig. 1A) inside the MRI environment with concomitant tTIS (please see Fig. 1B), either iTBS, cTBS, or control (each condition applied twice in a pseudo-randomized manner). Each block of the task started with a 2.5-min encoding phase during which participants had to memorize the location of three task objects in the virtual arena. This was followed by a retrieval phase, during which each object was presented to the participants one after another. They had to recall the original location of the cued task object and navigate to the retrieved location (i.e., retrieval trial). These trials were repeated multiple times, with each task block lasting a total of 9 min.

Our first aim was to investigate differential effects of iTBS and cTBS on behavioral performance during the spatial navigation task compared to the control. Statistical analysis was performed on raw data by using mixed-effects models, and visualization is presented normalized to the control condition to better depict the within-subject effects of the two active conditions, which could have been obscured by high inter-subject variability (*53*). Notably, we found a significant effect of the stimulation condition on retrieval time—the time participants spent in the retrieval phase of each trial ($F_{2,2745} = 3.10$, $P = 0.045$). The effect was driven by a significantly shorter trial time in the iTBS condition compared to the cTBS condition (Fig. 2A; $t_{2745} = 2.42$, $P = 0.04$, $d = -0.11$), suggesting higher temporal efficiency. Because the navigation velocity was fixed during the task, the shorter trial time could be due to (i) a shorter navigation path and/or (ii) a reduced delay until the participants started actively navigating (i.e., departure time). Stimulation conditions significantly affected the latter ($F_{2,2745} = 7.37$, $P < 0.001$), with the participants departing earlier during iTBS than cTBS (Fig. 2B; $t_{2745} = 3.79$, $P < 0.001$, $d = -0.18$) and even control ($t_{2745} = 2.42$, $P = 0.04$, $d = -0.11$), while we did not find a significant difference in navigated distance per trial (Fig. 2C; $F_{2,2745} = 0.43$, $P = 0.65$). The net trial time after the first departure did not differ across conditions ($F_{2,2745} = 0.59$, $P = 0.55$), confirming that shorter retrieval trials in the iTBS were due to earlier departure time and not shorter navigations. The distance over time from cue presentation to location selection is plotted in fig. S1. During the iTBS condition, the distance decreases faster, indicating that reduced departure times are more likely to be explained by a faster recall of the object position instead of impulsivity or arousal. Compatible with such specific behavioral effects on the memory recall, we also did not find a significant difference in actual navigation

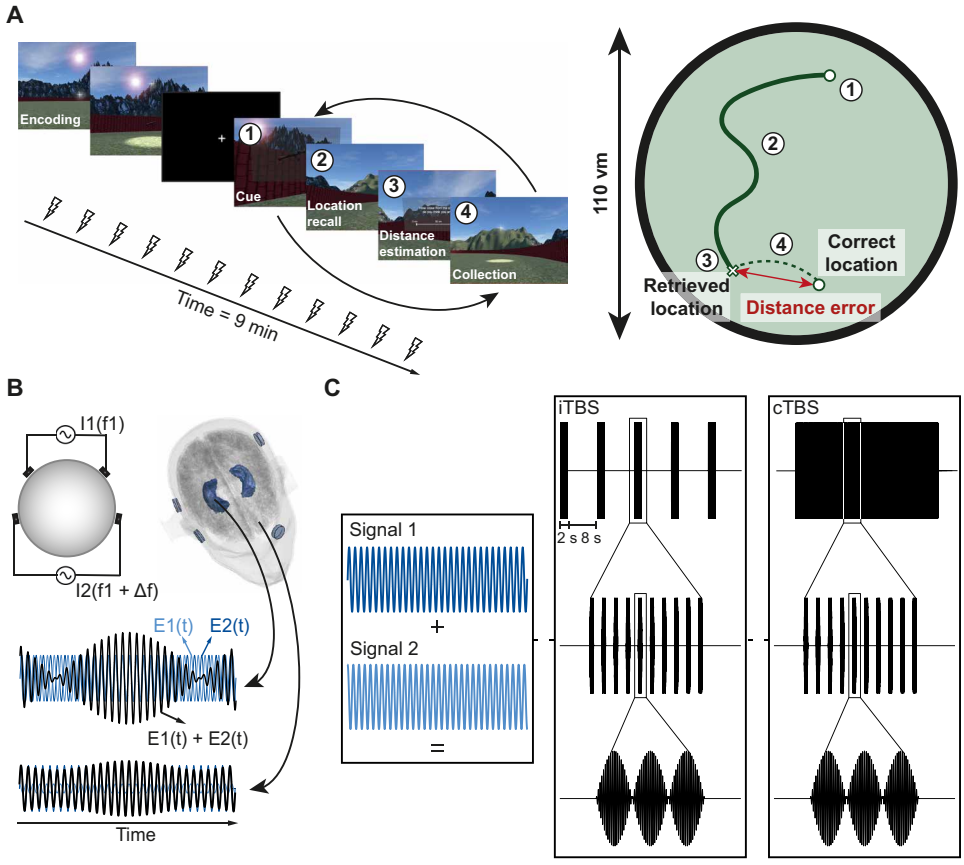

Fig. 1. Set-up of the experiment. (**A**) Spatial navigation task. Each block started with an encoding period during which participants were consecutively presented with three objects at specific locations and asked to memorize their position. After encoding each object multiple times, a cue was shown during the retrieval phase with the image of one of the objects and the participant had to navigate to the location of the object. (**B**) Temporal interference stimulation concept. Two pairs of electrodes are placed on the head and deliver two HF currents I1 and I2 at a frequency f1 and f2 = f1 + Δf, respectively. On the bottom of the panel, the combination of the two fields is shown with high envelope modulation inside the target region and low envelope modulation outside. (**C**) Theta burst protocols. A specific shift in frequency between the two signals was applied with a specific timing to mimic either iTBS or cTBS. During iTBS, central panel, trains of 2 s are applied every 10 s, each one composed of 10 bursts at 5 Hz. Each burst is composed of three pulses at 100 Hz. In the 8-s break, no shift is applied between the two sources, leading to a flat envelope. During cTBS, bursts at 5 Hz are applied continuously without breaks. The bursts are composed of three pulses at 100 Hz as for the iTBS protocol.

time during the encoding phase across the conditions ($F_{2,148} = 1.33$, $P = 0.27$). Possible carry-over effects were studied and showed that differences in departure time cannot be driven by the previously applied stimulation conditions (more information in text S2). In addition to the temporal aspect of navigation performance, we assessed the effect of tTIS on distance error (i.e., the distance between the recalled location and the correct location), which represents the accuracy of spatial memory. Distance error did not differ across the three conditions (Fig. 2D; $F = 0.41$, $P = 0.66$), indicating that reduced trial time in the iTBS condition cannot be explained by a shift in the speed-accuracy trade-off function. In addition, we could not find a significant relationship between trial time and the distance error ($F = 1.40$, $P = 0.23$). Of note, our participants were instructed to perform the task as accurately as possible but were not specifically instructed in terms of speed. These results suggest a facilitation in spatial navigation during the iTBS condition.

tTIS targeting HC-EC decreased GCLR with respect to control

We investigated brain activity changes associated with the tTIS targeting the right HC-EC, which might account for the navigation performance changes we observed (i.e., departure time). Given our hypothesis that GCLR in EC is closely related to spatial cognitive processes during the spatial navigation task, we calculated and compared GCLRs across the stimulation conditions. First, we assessed GCLR during the control condition and found that GCLR was significantly higher than 0 ($n = 28$, $r = 0.48$, $P = 0.009$), suggesting that hexadirectional grid codes were engaged during the task in the control condition. This result was in line with previous GCLR studies using similar tasks (*22*, *23*) including our own work using the exact same VR setup and scanner (*53*). The typical GCLR activity in the control condition suggests that our control condition does not influence the task-related entorhinal GCLR activity. Then, we assessed possible influences of the two active tTIS conditions on entorhinal GCLR activity by calculating GCLRs during these conditions and comparing them to the GCLR during control (Fig. 3A). We found that the magnitudes of GCLR were significantly decreased both in iTBS ($n = 28$, $r = 0.72$, $P < 0.001$) and in cTBS ($r = 0.39$, $P = 0.019$), with respect to control. Consistently, GCLR was not significantly greater than 0 in the iTBS ($n = 28$, $r = 0.42$, $P = 0.99$) and in the cTBS condition ($n = 28$, $r = 0.049$, $P = 0.40$), unlike the control condition.

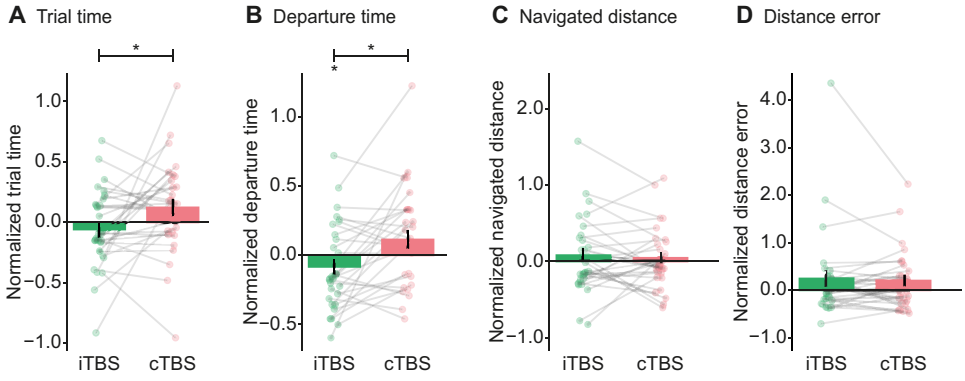

Fig. 2. Changes in the behavioral performance associated with tTIS targeted on the right HC-EC. For the visualization of the behavioral performance, the participant-wise mean per active TBS conditions was normalized with respect to the data in the control condition to better depict within-participant effects of the active stimulations. Normalization was performed using the Z score with the mean and standard deviation (SD) of the control data, i.e., (X - mean_ctrl) / sd_ctrl. Hence, a value of "0" on the *y* axis represents the control level (mean_ctrl). However, the statistical assessment was performed using the dedicated mixed-effect models with the trial-wise data points before normalization, and showed a significant difference for the trial time and departure time. $N = 30$. Barplots height indicates the mean and black lines show the standard error (SE). Asterisks represent significant differences with a P threshold of 0.05. (**A**) The time the participants spent per trial was shorter in iTBS than cTBS ($P = 0.04$). (**B**) Further analysis on departure time (i.e., time duration until a participant started actively moving) revealed that shorter retrieval trial time in iTBS than cTBS stemmed from the shorter departure time in iTBS (compared to cTBS, $P < 0.001$; compared to control, $P = 0.04$). There was no significant difference between conditions in (**C**) navigated distance per trial (possibly reflecting an efficiency of the navigation path) nor in (**D**) distance error (i.e., distance between the correct and recalled location, inversely indexing a precision of spatial memory).

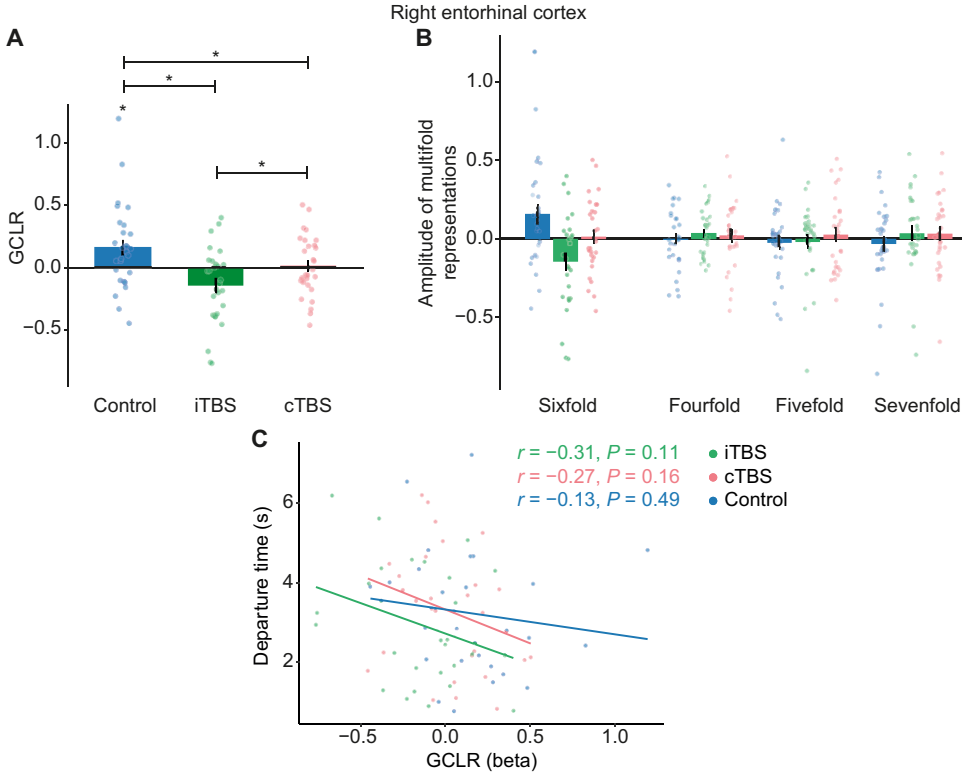

Fig. 3. Changes in the GCLR associated with the tTIS targeted on the right HC-EC. $N = 28$. Barplot height indicates the mean, and black lines show the SE. Asterisks represent significant differences with a P threshold of 0.05. (**A**) GCLR was significantly greater than 0 in the control condition ($P = 0.009$). Contrarily, GCLR was not greater than 0 in iTBS ($P = 0.99$) and in cTBS ($P = 0.40$). GCLR during the control was greater than GCLR during both iTBS ($P < 0.001$) and cTBS ($P = 0.019$). GCLR in iTBS condition was even lower than GCLR in cTBS condition ($P = 0.030$). (**B**) As a control analysis, we assessed other multifold symmetries (four, five, and sevenfold) than sixfold [i.e., GCLR results in (A)]. We found that only sixfold symmetry in the control condition was significant, confirming the validity of our GCLR data. (**C**) Correlation analysis between departure time and GCLR for each stimulation condition. No significant correlation was found.

However, we also found that GCLR during iTBS was lower than during cTBS ($r = 0.36$, $P = 0.03$). Of note, the symmetry in heading direction–dependent blood oxygen level–dependent (BOLD) signal was found only for sixfold (Fig. 3B) and not for the control symmetries (four, five, and sevenfold), and we did not find any significant GCLR in any of the conditions for the left EC (more information in text S3), further confirming the validity of our GCLR results. These data provide evidence that active tTIS in the form of TBS targeting the HC-EC complex alters the hexadirectional code (i.e., grid cell–like activity) in the EC, with differential changes depending on the applied protocol (iTBS versus cTBS).

We next assessed whether the difference in GCLR induced by the TBS conditions could account for the changes in departure time. To assess the relationship between the behavioral performance (departure time) and GCLR, we calculated the Pearson correlation between the two for each condition. There was no significant correlation in any of the conditions (Fig. 3C; $n = 28$, $r = -0.27$, $P = 0.16$ for iTBS; $r = -0.31$, $P = 0.11$ for cTBS; $r = -0.13$, $P = 0.49$ for control). No correlation was also found between GCLR and the other behavioral variables (more information in text S4 and fig. S5). To better assess the within-participant effect of the tTIS on both departure time and GCLR, we additionally calculated the correlations with the participant-wise differences of those data between each condition pair. Again, we did not find a significant correlation between the magnitude of the changes in GCLR and departure time in either of the condition comparisons ($n = 28$, $r = -0.12$, $P = 0.56$ for iTBS-control; $r = -0.07$, $P = 0.73$ for cTBS-control; $r = -0.05$, $P = 0.80$ for iTBS-cTBS). These results suggest that the magnitude of GCLR changes induced by active TBS might not be associated with the effect of the TBS on the behavioral performance (i.e., shortened departure time). Furthermore, they indicate that the effects of tTIS on spatial navigation cannot be solely accounted for by changes in grid cell–related activity. Instead, other brain mechanisms may b modulated by tTIS targeting EC-HC.

Effect of stimulation on departure time was associated with hippocampal BOLD activity

Following the GCLR analysis, we investigated other neural correlates of the behavioral effects induced by tTIS. For that purpose, we analyzed whether tTIS affects BOLD activity at the whole-brain level. As a first step, the regions more involved during active navigation (i.e., the periods when participants actively navigated in the virtual arena, during which GCLR is generated) compared to stationary periods were derived [generalized linear model (GLM) analysis] for the control condition. As expected, bilateral motor regions such as the left supplementary motor area and left precentral gyrus, as well as spatial navigation regions such as the right precuneus and lingual gyrus [in the calcarine or superior parietal cluster (*57*)], showed navigation-related activity (all significantly activated regions are reported in table S1). We then investigated possible stimulation effects on different cognitive modes: active navigation and Cue+Retrieval periods. Cue+Retrieval included the time between the appearance of the cue to retrieve until the report of the recalled position, i.e., the phase of recalling the information about the object position and its retrieval. We implemented a flexible factorial design with subject, stimulation, and block as factors and computed t tests on the contrasts between the stimulation conditions. No significant differences were found in these analyses, indicating that active tTIS did not induce significant changes in the BOLD activity in whole-brain analysis.

In a second analysis, we extracted the activity within the right HC and the right EC separately to investigate stimulation-related effects on the targeted regions (Fig. 4A). We ran a linear mixed-effects model with stimulation, cognitive mode (active navigation versus Cue+Retrieval period), and regions of interest (ROI) as fixed factors and participant as random factor. We found a significant effect of the cognitive mode ($F_{1,319} = 82.84$, $P < 0.001$, $P\eta^2 = 0.21$) due to higher activity during the Cue+Retrieval periods and of the ROI ($F_{1,319} = 13.98$, $P < 0.001$, $P\eta^2 = 0.04$) due to higher hippocampal activity with respect to EC, together with a significant interaction between cognitive mode and ROI ($F_{1,319} = 12.61$, $P < 0.001$, $P\eta^2 = 0.04$). The interaction was driven by a significantly higher activity within the hippocampus with respect to the EC during the Cue+Retrieval periods ($t_{319} = -5.155$, $P < 0.001$, $d = -0.77$) but not during active navigation ($t_{319} = -0.13$, $P = 0.89$, $d = -0.02$). No stimulation effects were found ($F_{2,319} = 1.39$, $P = 0.25$, $P\eta^2 < 0.001$). This highlights a greater involvement of the right HC during the Cue+Retrieval period with respect to the right EC, independent of the concomitant stimulation condition.

On the basis of the greater hippocampal activation during Cue+Retrieval, we then focused on this region to determine its possible impact on spatial navigation behavior. In particular, we aimed at exploring whether right hippocampal BOLD activity may underlie behavioral differences between iTBS and cTBS, which GCLR did not account for. To do so, we computed the correlation between the departure time and both Cue+Retrieval and active navigation–related BOLD activity. As the departure time (altered by iTBS; see Fig. 2B) is within the Cue+Retrieval phase, any significant effect would be expected during this phase, but not during the general active navigation phase. In line with this, we found a significant correlation ($r = -0.55$, $P = 0.01$) between the difference in departure time and the difference in Cue+Retrieval BOLD activity in the right HC between iTBS and cTBS (Fig. 4B). This was not the case for the active navigation–associated activation ($r = 0.06$, $P = 0.75$). The significant reduction of the departure time induced by iTBS is hence associated with systematic differences in right hippocampal brain activity, specifically during the Cue+Retrieval period, compatible with faster retrieval of the information about the object location. These findings show that faster departure time in iTBS compared to cTBS, not accounted for by GCLR changes, is associated with differences in right hippocampal activity between the two active TBS conditions. As an additional control, no correlation was found when investigating activity in motor-related areas as described in text S6.

Control conditions showed no differential effects on behavior

To better support the assumption that HF and sham control can be merged as a single control condition, we compared behavioral results between the first half of the participants ($n = 16$) who received HF control stimulation versus the second half of the participants ($n = 14$) who received sham stimulation. Permutation tests (10,000 repetitions) were performed, randomly assigning the participants to one or the other group to create a probability distribution of the difference between the two groups of the behavioral variables for each stimulation protocol (iTBS, cTBS, and control). We then computed the probability of observing a greater difference than the real one based on that probability distribution. For the distance error, the probability of obtaining a difference greater than the one observed between the two groups was $P = 0.0087$, $P = 0.008$, and $P = 0.0002$

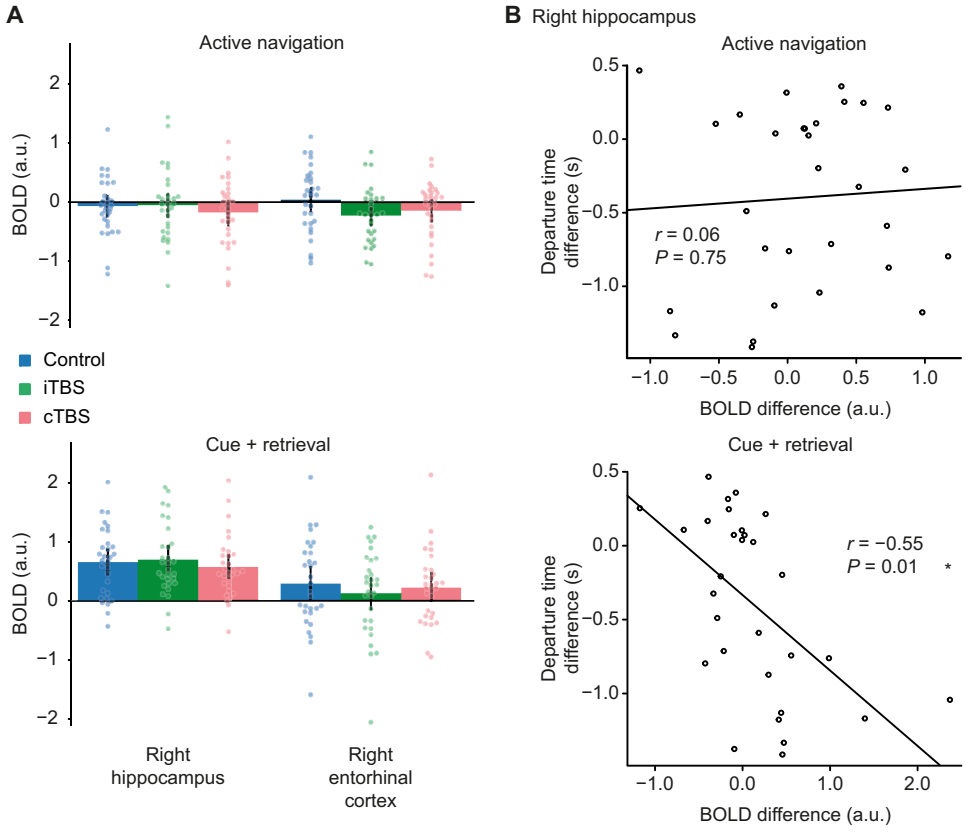

Fig. 4. Extracted BOLD activity in target areas. $N = 30$. Barplot height indicates the mean and black lines show the 95% confidence interval. (**A**) Average BOLD activity within the right hippocampus (left barplots) and the right entorhinal cortex (right barplots) during each stimulation session. In the top and bottom panels, activity associated with active navigation periods and with Cue + Retrieval periods are plotted, respectively. (**B**) Correlation between the difference in departure time versus the difference in averaged BOLD activity within the right hippocampus between iTBS and cTBS. A significant correlation was found during Cue + Retrieval (bottom, $r = -0.55$, $P = 0.01$), indicating that the higher the BOLD activity during iTBS versus cTBS is, the faster the participants were recalling the position of the object to start navigation. No significant correlation was found during active navigation (top, $r = 0.06$, $P = 0.75$). a.u., arbitrary unit.

for iTBS, cTBS, and control conditions, respectively. Selecting a threshold of 0.05 to establish whether the difference was significantly different than a random distribution, the two groups showed a significant difference in distance error. Because of the comparable probabilities in all of the three conditions, we conclude that the difference is not driven by the control stimulation (HF versus sham). We repeated the same analysis on the departure time, and we obtained a probability of $P = 0.1189$, $P = 0.0584$, and $P = 0.0571$ for iTBS, cTBS, and control conditions, respectively. Again, although iTBS seems to display a higher probability of observing differences more extreme than the other two stimulation protocols, the presence of a marginally significant difference in both cTBS and control stimulation leads to the conclusion that the two controls did not drive a behavioral difference, supporting the validity of combining the groups. In addition, we tested whether there was a significant difference between the performance changes from the control condition to the active conditions depending on which control condition a participant received. As it can be seen in Fig. 5, there were no significant differences between the two control groups in both distance error (Wilcoxon rank-sum exact test, iTBS versus control: $W = 101$, $P = 0.667$; Welch two-sample t test, cTBS versus control: $t_{22.3} = 0.19$, $P = 0.85$) and departure time (Welch two-sample t test, iTBS versus control: $t_{27.7} = -1.07$, $P = 0.29$; Welch two-sample t test, cTBS versus control: $t_{25.5} = -0.03$, $P = 0.98$), when comparing iTBS or cTBS minus HF performances and iTBS or cTBS minus sham performances.

DISCUSSION

This study aimed to investigate the causal role of the HC-EC for spatial navigation in humans by testing whether noninvasive deep brain stimulation by means of tTIS can modulate the right HC-EC complex during a spatial navigation task and consequently affect navigation behavior. At the behavioral level, we found that hippocampal iTBS stimulation facilitated spatial navigation leading to faster departure times as compared to the cTBS condition. Such faster departure times did not come at the cost of navigational accuracy. fMRI analyses showed that entorhinal GCLR was significantly weakened in both iTBS and cTBS compared to the control, with the GCLR in iTBS even lower than in cTBS. However, the stimulation-induced changes in entorhinal GCLR did not fully account for the changes in navigation behavior (i.e., departure time), suggesting that additional brain mechanisms, affected by TBS, were underlying the navigational behavioral change. Our fMRI analysis detected these in an MTL area outside the EC, in the right HC, by showing that right HC activity significantly correlated with navigational changes (departure time differences) when comparing iTBS versus cTBS.

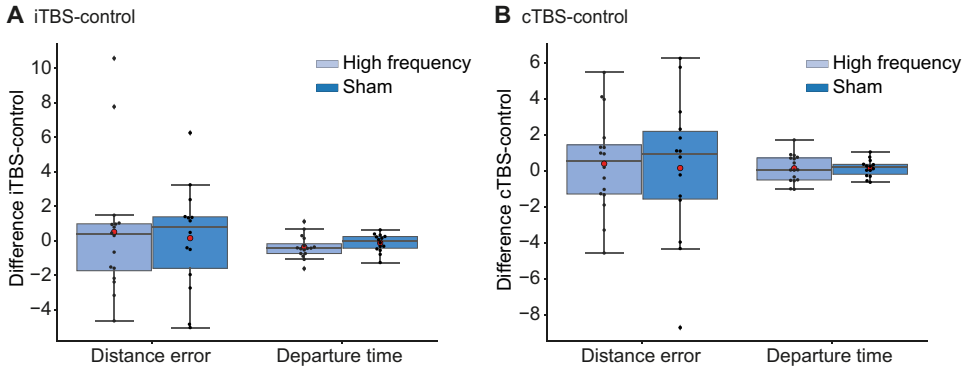

Fig. 5. Sham versus HF control stimulation. $N = 30$. Comparison of the differences between active and control conditions, HF versus sham, in behavioral performance (distance error and departure time, respectively). On the left (**A**), the iTBS versus control conditions is shown, while on the right (**B**), cTBS versus control conditions is plotted. No significant difference was observed between the two controls. In all box plots, the middle horizontal line represents the median value, while the red dot represents the mean value, colored areas represent the interquartile range, and the whiskers represent the 1.5 interquartile range.

Our results demonstrate that iTBS of the right HC-EC improved spatial navigation performance, characterized by shorter trial time compared to cTBS. Further analyses revealed that reduced delay time before active navigation (i.e., departure time) rather than a more efficient (i.e., shorter) navigation path accounted for the reduced trial time in iTBS versus cTBS condition. Of note, the departure time in iTBS was also shorter than in the control condition, suggesting an overall facilitation of spatial navigation function through direct electrical stimulation of human HC-EC regions. However, we found no effects of TBS on either distance errors (indexing spatial memory precision) or on navigated distance per trial (reflecting efficiency of spatial navigation). These results suggest that the facilitatory effect of iTBS on HC-EC induces faster recall of spatial information rather than other spatial cognitive processes during the navigation task. The change in behavior that we observed might not necessarily be enhanced spatial memory. However, it is of note that improvement in trial time was not at the cost of reduced accuracy. Hence, the present results cannot be accounted for by a shift in the speed-accuracy trade-off curve toward higher speeds [as demonstrated in other cognitive domains (*58*–*60*)]. If the participants reach the target faster without any decrease in spatial accuracy, we consider this change a facilitation in spatial navigation behavior. Therefore, we argue that faster departure times and, in turn, reduced overall time to reach the destination in iTBS condition indicate improved behavioral performance during spatial navigation. One could argue that the earlier departure in the iTBS condition might be derived from either an increase in confidence or changes in decisional processes in this condition. However, our data do not support these alternatives as described in text S7. This is in line with a recent study by Basu and colleagues (*61*), who also reported faster cognitive processing associated with invasive stimulation of the internal capsule without any reported effects on confidence.

In humans, previous studies investigating the causal role of the HC-EC complex in spatial navigation were limited to invasive techniques in patients, applying invasive electrical stimulation of deep brain structures in patients with epilepsy via electrodes implanted for medical reasons. Contrasting results were reported, with 50 Hz of stimulation leading to either improved (*29*) (variable stimulation duration with repetition of 5-s on/off trains) or impaired accuracy of spatial memory (10 s) (*30*, *31*). In the present study, we report improvements of departure time, a different aspect of spatial navigation (compared to previously reported measures). Such different effects could be explained by various differences in the design of the experiments, such as stimulation target, stimulation protocol, duration and intensity, or characteristics of the task. Furthermore, past studies focused on patient cohorts because of the possibility of using invasive electrodes, while tTIS allowed us to study spatial navigation in healthy individuals using NIBS. In implanted patients, the targets can vary even within the same study, being affected by clinical decisions to target the right and/or left side of HC-EC as well as anterior or posterior regions (*29*–*31*). In contrast, for tTIS, the stimulation exposure target is wider and can be designed to be more homogeneous across participants. Stimulation duration and intensity also changed between these previously mentioned invasive studies and is another important difference with respect to the current protocol. Here, tTIS was delivered during both encoding and retrieval periods, while in previous works, the stimulation was restricted to the encoding (*29*–*31*). Current intensities are difficult to compare since (i) stimulation was delivered at the level of the scalp versus intracranial depth electrodes directly placed in the targeted structures, and (ii) exposure field magnitudes are not directly comparable with field modulation magnitudes. Of note, an additional difference introduced in our study is the application of theta burst–patterned stimulation, an LTP-inducing protocol, in contrast to the 50-Hz stimulation in the aforementioned studies. While current results are in line with the conclusion that the HC-EC complex is functionally relevant in spatial navigation functions, discrepancy to previous work in patients in terms of behavioral results might be related to the differences in the experimental design and stimulation parameters outlined above, as well as the different cohorts tested.

In the current study, we observed that both TBS conditions significantly decreased entorhinal GCLR, which was prominent in the control conditions. This adds to the current knowledge by showing modulation of GCLR via stimulation of deep brain structures (i.e., HC-EC). Furthermore, it supports the hypothesis that tTIS is able to reach deep structures—in particular, the right HC-EC—and demonstrated for the modulation of spatial navigation behavior. Our results further link the characterized grid cell–like signals to processes in the HC-EC, demonstrating that even subthreshold electrical stimulation of HC-EC can alter the grid code when the target region is

engaged in a task. The hexagonal firing fields of grid cells (i.e., grid code) have been proposed to originate from the delicately tuned interconnection of multiple neurons in the regions based on rodent studies (*62*, *63*). Supporting the idea also in humans, we found that GCLR decreased when excitability of the cells in HC-EC was altered by active TBS stimulation. In contrast, intact GCLR patterns observed in the control condition strongly suggest that HF electrical field without temporal interference did not interrupt the delicate neural circuits, confirming the spatial selectivity of tTIS targeting the deep brain. However, nonsignificant GCLR based on fMRI should be carefully interpreted (*22*) because either shearing-induced asymmetry (*64*) or unstable grid orientations (*22*, *23*, *53*), as well as the actual disappearance of the grid cell–like activity can lead to weaker fMRI-based GCLR. Thus, further follow-up studies using depth electrodes in MTL are required to scrutinize the GCLR changes we observed.

At first glance, the decreased GCLR induced by iTBS compared to the control and even to cTBS seems unexpected, as we observed improved behavioral performance in iTBS. However, several previous studies reported that GCLR magnitude was not directly related to spatial navigation performance in similar navigation tasks (*23*, *25*, *53*, *65*). In these studies, decreases of GCLR have been linked to the equivalent or even improved spatial memory/navigation performance, compatible with the findings of the present study. Kunz *et al.* (*23*) suggested that hippocampal activity may be a compensatory mechanism related to reduced GCLR in healthy participants with a genetic-risk factor [apolipoprotein E-ε4 (APOE-ε4)] for Alzheimer's disease, allowing them to maintain spatial navigation precision equivalent to healthy non-ApoE carriers. In line with this observation, it could be speculated that the positive correlation between hippocampal activity and departure time (Fig. 4B) could be due to this compensatory hippocampal recruitment. We found that higher activity within the HC was associated with a faster performance during iTBS with respect to cTBS, although iTBS showed a reduced GCLR with respect to cTBS. It should be noticed that in our initial hypothesis, we expected opposite effects of iTBS versus cTBS conditions based on initial literature on these protocols (*52*). However, while this holds true for behavioral changes, which showed opposite trends, the reduction of GCLR in both conditions could be explained by specific stimulation parameters. Recent studies demonstrated how effects of TBS protocols also depend on dose and intensity (*66*) as well as on interindividual differences (*67*).

The correlation between hippocampal activity and departure time was only observed during the Cue+Retrieval phase, but not during the active navigation phase, suggesting that this period is more strongly affected by the tTIS. Most previous studies investigated correlations between hippocampal activity and spatial navigation performance measured by navigation accuracy or the distance error (*68*, *69*), while the trial time or departure time have rarely been examined. However, it was also shown that after the initial exploration period, which highly depends on the hippocampus, during retrieval, the hippocampus is again engaged in the planning of goal-directed navigation by representing prior spatial elements (*70*). This is used in the planning or alterations of routes during the initial part of the retrieval process (*71*, *72*). Therefore, one could speculate that the iTBS led to a faster recall of the location of the target and/or a faster navigation planning by simultaneously having a dual effect on grid cells and hippocampal activity. Accordingly, iTBS would lower GCLR while increasing hippocampal activity, which was associated with the reduced departure time compared to the cTBS. A possible mode of action of the TBS protocol could rely on the pyramidal cells of the hippocampal subregion CA1, which show an *N*-methyl-D-aspartate receptor–dependent LTP-like plasticity, mediating spatial navigation functions (*73*, *74*). Moreover, stimulation of CA1 and CA3 was directly shown to modulate place cell activity (*75*) and support place cell stability (*76*). In addition, LTP can result in a modulation of behavior-related firing without acting on the global firing rate (*75*). The neural effects of iTBS and cTBS observed in the present study, on GCLR and BOLD, could potentially be explained by a rearrangement of HC-EC circuits by LTP or LTD-like plasticity. This may account for the observed behavioral modulation despite the lack of significant changes in the averaged hippocampal BOLD activity.

The current study presents some limitations that should be considered for interpretation of the results. As mentioned above, the experiment was not conceived for a block design analysis and both BOLD and generalized psychophysiological interaction (gPPI) analysis considered either active navigation or Cue+Retrieval periods as blocks. This implies that the activity during these phases was not compared to a traditional resting period and could hence hide activation of regions already partially engaged between the blocks. Future studies not investigating GCLR should be adapted to better studying tTIS effects on hippocampal complex activity. In this case, more specific research questions could be addressed, such as differences between encoding and retrieval periods. Previous studies in fact show a differential engagement of the anterior and posterior MTL based on spatial navigation phases and conditions (*54*, *77*), as well as differential effects of stimulation depending on which phase was targeted (*78*). Hence, it would be interesting to further investigate whether tTIS could be steered to support the respective role of each subcompartment. An additional limitation of the current results, although promising, is that they do not provide direct evidence of a focal effect of the stimulation since no changes in conventional BOLD signal level were found in the target region alone. This could be due to either the current study design or to a low focality of the stimulation. Because the same montage (mirrored between right and left) was demonstrated to focally reach the hippocampus in the work from Violante *et al.* (*37*), the first explanation seems more likely. However, the question about focality remains open, with several aspects that could be further optimized. First, the electrode locations have been chosen by modeling the tTIS fields on a head template. Personalized modeling that considers the subject-specific anatomy could help identify personalized stimulation conditions, potentially resulting in superior outcomes (*28*, *79*). Second, several studies showed that increasing the number of electrode pairs could also significantly improve focality (*80*–*84*). Last, we note that the control condition was changed, with the first 16 participants receiving HF stimulation without any shift, while the last 14 received sham stimulation (5-s ramp-up followed by 5-s ramp-down). However, there is now substantial evidence that these two control conditions are equivalent (*85*) and lead to comparable sensations, thus ensuring good blinding. On the basis of previous studies, neural and behavioral effects are also comparable, and, since the main behavioral difference was found between iTBS and cTBS, the change of control is not expected to influence the interpretation of the current results.

After taking all the considerations reported above, this study reports (i) improved navigation behavior induced by iTBS (versus cTBS) stimulation of the HC-EC complex by accelerating the departure time during the retrieval of a spatial navigation task, (ii) lower entorhinal GCLR activity, as well as (iii) higher right hippocampal

activity corresponding to faster performances when compared to cTBS. Further animal and human research is needed to advance our understanding of these delicate MTL circuits and their involvement and noninvasive modulation in spatial navigation.

Overall, the current study provides further evidence for the feasibility of noninvasive focal neuromodulation of deep brain structures by means of tTIS. This was achieved via combining fMRI and MR-compatible immersive VR to the stimulation technology. It allowed us to investigate a causal link between a very crucial daily life behavior (i.e., spatial memory/navigation) and the changes in neural activities corresponding to noninvasive stimulation of the right HC-EC. As a result, we showed successful modulation of the HC-EC while the participants were engaged in a spatial navigation task. Critically, the tTIS-induced brain changes were associated with behavioral effects in spatial memory/navigation that were dependent on the stimulation protocol used. Our findings have implications for translational neuroscience because changes in spatial navigation behavior are observed in the early stage of neurodegenerative pathologies such as Alzheimer's disease (*86*, *87*). Successful modulation of deep brain structures critically involved in spatial navigation behavior, as reported here, sets the ground for future studies translating the present neurotechnology toward innovative noninvasive interventional treatment strategies.

MATERIALS AND METHODS

Participants

Thirty young healthy individuals were enrolled in the current study (right-handed, 16 females, 23.63 ± 4.07 years old). The participants were naive to the purpose of the investigation and gave their informed consent following the Declaration of Helsinki (2013). The study was approved by the Cantonal Ethics Committee Vaud, Switzerland (project number 2020-00127). Inclusion and exclusion criteria are detailed in text S8.

Transcranial temporal interference electric stimulation

tTIS was applied as low-intensity transcranial electric stimulation via two isolated constant current sources (DS5 Isolated Bipolar Constant Current Stimulator, Digitimer, Letchworth Garden City, UK) (*32*, *88*). The electrodes montage was adapted from Violante *et al.* (*37*), inversing right and left electrodes to target the right hippocampus. The final montage consisted of two pairs of electrodes placed in proximity to the P7-CP8 and Fp1-FT8 EEG 10-20 electrode positions (*89*). This previous study demonstrated that the chosen montage allows the focal targeting of the hippocampus, with evidence coming from both computational modeling on a template brain and human cadaver measurements (*37*). Because of the symmetrical montage and to support the adopted montage, we additionally plotted field distribution within the targets and control regions based on the closest EEG 10-20 electrode positions, confirming good focality of the stimulation (fig. S6). The following stimulation parameters were applied: sinusoidal waveform; current intensity per channel, 2 mA (baseline to peak); carrier frequency, 2 kHz; fade-in/out interval, 5 s; 3 cm^2 circular conductive rubber electrodes with conductive paste. The participants received three different stimulation protocols: iTBS, cTBS, or a control stimulation. The first two patterned stimulation protocols (*52*, *90*, *91*) (see Fig. 1C) were achieved by applying a frequency shift in a time-precise manner [as in a previous work (*35*)]. This frequency shift created the same basic element, which was a stimulation burst composed of three envelope-modulated sinusoidal pulses at 100 Hz. Because the pulses resulted from the shift in frequencies between the two electrode pairs, each pulse had an HF component equal to the average between the two HFs, which is suggested to not influence neuronal activity (*32*, *35*–*37*). The shift was introduced at specific intervals to create the burst at a frequency of 5 Hz. While in the iTBS protocol, bursts were delivered for 2 s (train) every 10 s, and cTBS was characterized by continuous delivery of bursts (still at a 5-Hz frequency). The control stimulation consisted in pure kilohertz-frequency stimulation without any frequency shift, hence resulting in a flat envelope (*35*). Sixteen individuals received the control during the whole duration of the task, while 14 of them received it for 10 s at the beginning of the task (ramp up and ramp down only). The two controls were demonstrated to be equivalent in terms of safety and blinding effects (*85*). Furthermore, additional proof on the null effects of HF, similar to sham, was shown on motor evoked potential (MEP) amplitudes and BOLD activity directly underneath the electrodes (*35*–*37*). An impedance check was performed right after placement of the electrodes, right before the beginning of the task, and at the end to verify good contact between electrodes and skin. A sensation test was performed before the beginning of the task to familiarize the participants with the current sensation (more information in text S10). Each of the three protocols was applied starting with a current of 0.5 mA baseline-to-peak per channel and gradually increased until 2 mA with a step of 0.5 mA. The participants were asked to report any kind of sensations and to evaluate the strength (mild, moderate, or strong) and the type of sensation.

MRI-compatible VR spatial navigation task

The task program was adapted from the task used in the previous work of Moon *et al.* (*53*). The task procedures, task arena, and task objects were implemented with Unity 3D Engine (Unity Technologies). During the task, only distal landmarks were placed outside of the circular task arena, providing orientation cues. The visual input was provided through MRI-compatible stereoscopic VR goggles (NordicNeuroLab: 1920 × 1200 resolution per eye, 60-Hz refresh rate). The participants manipulated an MRI-compatible button box (Fiber Optic Response Pad, Current Designs) to perform the task in the scanner.

During each round, the participants underwent a 9-min spatial navigation task while being stimulated in MRI. The task consisted of two phases: encoding and retrieval (Fig. 6). In the encoding phase, the participants memorized the locations of three objects within the arena for 2.5 min. After encoding, the participants performed the memory retrieval trials for approximately 6 min until the stimulation ceased and the experimental round was ended. Each trial began with a cue, indicating the target object, and the participants had to recall its encoded location and navigate back to the location where they remembered the object was placed. Upon reaching the retrieved location, the participants pressed a button to confirm the answer and estimated the distance error they made. As feedback, the target object appeared at the correct location, and the participants had to navigate to and collect it so that they could continue to the next trial. Written instructions were provided before the experiment, asking the participants to perform "as accurately as possible." Various spatial navigation performance (e.g., distance from the correct and retrieved location, navigation departure time, and navigated distance and time) were assessed through the parameters recorded during the task.

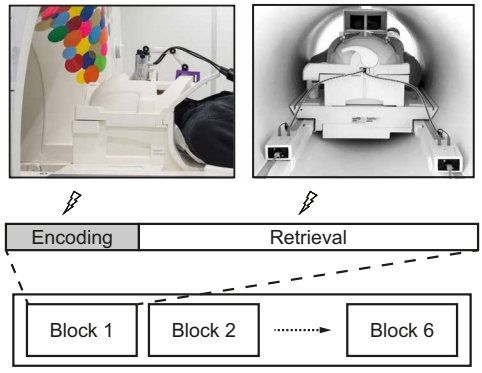

Fig. 6. Protocol of the experiment. During the single session, each participant performed six blocks of the spatial navigation task with stimulation applied during the whole duration of the task. Stimulation conditions were applied twice in a pseudo-randomized order A-B-C-C-B-A.

In total, each participant went through six task rounds with the three stimulation conditions, in a pseudo-randomized order (A-B-C-C-B-A), which was also counterbalanced across participants (i.e., three conditions are randomly assigned to "A," "B," and "C" per participant). Both participants and experimenters were blinded for the condition at the time of data acquisition and data exclusion.

MRI data acquisition

The MRI data acquisition was conducted at the Human Neuroscience Platform of the Campus Biotech (Geneva, Switzerland) with a 3T MRI scanner (SIEMENS, MAGNETOM Prisma). The two structural images were acquired respectively with a T1-weighted MPRAGE sequence (1 mm–by–1 mm–by–1 mm voxels, TR = 2300 ms, TE = 2.25 ms, TI = 900 ms, number of slices = 208) and also with a T2-weighted sequence (0.8 mm–by–0.8 mm–by–0.8 mm voxels, TR = 3000 ms, TE = 409 ms, number of slices = 208). The fMRI images covering the whole cerebrum were acquired during the task with a T2*-weighted echo planar imaging sequence (2-mm isotropic voxels, TR = 1500 ms, TE = 30 ms, FoV = 224 mm, number of slices = 69, multiband factor = 3, GRAPPA = 2). To correct possible distortion of functional images by the inhomogeneous B0 field, both magnitude and phase maps of the B0 field were measured.

fMRI analysis

Preprocessing

fMRI data were preprocessed with SPM12 (https://www.fil.ion.ucl.ac.uk/spm/), in MATLAB R2018a. The preprocessing pipeline for functional images included slice-time correction, spatial realignment, unwarp based on the voxel displacement map, normalization to the standard Montreal Neurological Institute (MNI) space, and smoothing using a 5-mm isotropic Gaussian kernel. Preprocessing of the individual T1-weighted structural images included coregistration to the average functional image and tissue segmentation. Bias-corrected gray and white matter maps were extracted, and the created deformation field was used in the normalization step of the functional images. A quality check of the data and of the preprocessing results was performed via visual check of the images and by ensuring that less than 40% of voxels exceed a framewise displacement (FD) of 0.5. In addition, total signal-to-noise ratio (tSNR) maps were computed by dividing the average of the time series for each voxel by its SD. Comparison of the tSNR right under the electrodes versus locations further away was used to assess possible noise associated with the stimulation (more information in text S11).

T1w and T2w structural images were also preprocessed via the recon-all function of Freesurfer (v7.1.1, http://surfer.nmr.mgh.harvard.edu). The resulting parcellation in each individual space was then used to extract MTL ROIs of each participant (including HC and EC) based on the Desikan-Killiany Atlas (*92*) and cytoarchitecturally-defined entorhinal label. The automatically defined ROIs were manually examined, coregistered with the mean functional images and finally normalized to the MNI space.

Grid cell–like representation

The GCLR analysis was conducted in the native space without normalization, following previous studies (*23*, *25*, *53*). Of note, five rounds with max FD more than 3 mm (of total 168 rounds) and two participants who have three rounds (a half of the six scanning rounds per participant) over the threshold were excluded from the GCLR analysis. GCLR was calculated using the Grid Code Analysis Toolbox [GridCAT v1.03, https://nitrc.org/projects/gridcat (*93*)] running on MATLAB 2021b. The analysis was performed in line with the previously established method (*22*, *53*). Briefly, as the first step, a putative grid orientation was estimated with a portion of data. Then, on the basis of the estimated grid orientation (φ) and the heading-direction information, hexadirectional modulation was calculated by contrasting regressors for movement in grid-aligned direction (φ + 0, 60, 120, 180, 240, 300) versus misaligned direction (φ + 30, 90, 150, 210, 270, 330). The GCLR analysis was based on the leave-one-out cross-validation (*53*, *94*). Thus, GCLR per round was calculated with the grid orientation estimated from the other five scanning rounds. Then, condition-wise GCLRs were acquired by averaging the round-wise results by conditions. Three round-wise data points (of 652, including control analyses of the four/five/sevenfold symmetry; 0.46%) outside three SD range were excluded.

GLM analysis to detect task-related brain regions

Whole-brain GLM analysis was conducted with normalized and smoothed fMRI data using SPM12 to assess changes in response to the different stimulation protocols. Six motion regressors were generated from the realignment process (three for displacement and three for rotation) and included in the GLM, together with the white matter and corticospinal fluid normalized time series. In addition, ArtRepair toolbox (Art_Repair v5b3) was used to detect fMRI volumes with severe motion artifacts, which were also considered in GLM via additional regressors. For the block design, we defined two different vectors describing different aspects of the task: Cue+Retrieval and active navigation. As a second step, we also performed ROI-based analysis by extracting the average beta estimate within the individual hippocampal and entorhinal ROIs for each of the cognitive modes and stimulation protocol.

Statistical analysis

The differences in behavioral parameters were assessed with dedicated mixed-effects models using an R package (lme4, v1.1.26; https://R-project.org) running on R (v4.1.2 for Windows; https://R-project.org) and Rstudio (v2021.09.01; https://R-project.org). Random slopes were included unless the model failed to estimate. The data distribution of each dependent variable was assessed using a package of R (fitdistrplus, v1.0–11; https://R-project.org), to apply proper parameters for each mixed-effects regression. The statistical

assessments of GCLR data were performed using the Wilcoxon signed-rank test. A significance of GCLR (greater than 0) was assessed with a one-sided test based on a priori hypothesis, while difference of GCLRs between the conditions were assessed with a two-sided test. Inter-parameter relationships were assessed with the Pearson correlation. The GLM used for the whole-brain fMRI analysis was implemented with SPM12 (http://fil.ion.ucl.ac.uk/spm), and significant results were reported for voxel-wise uncorrected $P = 0.001$ and corrected $P = 0.05$ for cluster-wise false discovery rate (FDR) (if not specified otherwise). BOLD tests were performed using R (v4.2.2; https://R-project.org/). Linear mixed models were implemented with the lmer function [lme4 package (*95*)], and significance was assessed via the anova function of the lmerTest package (*96*) with Satterthwaite's approximations. For the BOLD analysis, stimulation (iTBS, cTBS, and control), cognitive mode (active navigation, Cue+Retrieval), and ROI were used as fixed factors and participant as random factor. Post hoc comparisons were tested when necessary by computing estimated marginal means via the emmeans package (*97*). The reported effect sizes were derived with the effectsize package (*98*). Last, the correlations between the different variables were computed with the corr.test function [psych package (*99*)] using the Pearson method with FDR for multiple comparison correction.

Supplementary Materials

This PDF file includes:

Supplementary Text
Figs. S1 to S8
Tables S1 and S2
References

REFERENCES AND NOTES

1. S. D. Moffat, Aging and spatial navigation: What do we know and where do we go? *Neuropsychol. Rev.* **19**, 478–489 (2009).
2. A. W. Y. Li, J. King, Spatial memory and navigation in ageing: A systematic review of MRI and fMRI studies in healthy participants. *Neurosci. Biobehav. Rev.* **103**, 33–49 (2019).
3. D. Head, M. Isom, Age effects on wayfinding and route learning skills. *Behav. Brain Res.* **209**, 49–58 (2010).
4. K. Vlček, J. Laczó, Neural correlates of spatial navigation changes in mild cognitive impairment and Alzheimer's disease. *Front. Behav. Neurosci.* **8**, 89 (2014).
5. J. Plácido, C. A. B. de Almeida, J. V. Ferreira, F. de Oliveira Silva, R. S. Monteiro-Junior, G. G. Tangen, J. Laks, A. C. Deslandes, Spatial navigation in older adults with mild cognitive impairment and dementia: A systematic review and meta-analysis. *Exp. Gerontol.* **165**, 111852 (2022).
6. E. Portegijs, M. Rantakokko, T. M. Mikkola, A. Viljanen, T. Rantanen, Association between physical performance and sense of autonomy in outdoor activities and life-space mobility in community-dwelling older people. *J. Am. Geriatr. Soc.* **62**, 615–621 (2014).
7. G. Cona, C. Scarpazza, Where is the "where" in the brain? A meta-analysis of neuroimaging studies on spatial cognition. *Hum. Brain Mapp.* **40**, 1867–1886 (2019).
8. M. Fricke, C. Morawietz, A. Wunderlich, T. Muehlbauer, C.-P. Jansen, K. Gramann, B. Wollesen, Successful wayfinding in age: A scoping review on spatial navigation training in healthy older adults. *Front. Psychol.* **13**, 867987 (2022).
9. A. D. Iordan, S. Ryan, T. Tyszkowski, S. J. Peltier, A. Rahman-Filipiak, B. M. Hampstead, High-definition transcranial direct current stimulation enhances network segregation during spatial navigation in mild cognitive impairment. *Cereb. Cortex* **32**, 5230–5241 (2022).
10. P. Byrne, S. Becker, N. Burgess, Remembering the past and imagining the future: A neural model of spatial memory and imagery. *Psychol. Rev.* **114**, 340–375 (2007).
11. W. B. Scoville, B. Milner, Loss of recent memory after bilateral hippocampal lesions. *J. Neurol. Neurosurg. Psychiatry* **20**, 11–21 (1957).
12. L. R. Squire, Memory and brain systems: 1969-2009. *J. Neurosci.* **29**, 12711–12716 (2009).
13. G. Buzsáki, E. I. Moser, Memory, navigation and theta rhythm in the hippocampal-entorhinal system. *Nat. Neurosci.* **16**, 130–138 (2013).
14. T. Hafting, M. Fyhn, S. Molden, M.-B. Moser, E. I. Moser, Microstructure of a spatial map in the entorhinal cortex. *Nature* **436**, 801–806 (2005).
15. E. I. Moser, E. Kropff, M.-B. Moser, Place cells, grid cells, and the brain's spatial representation system. *Annu. Rev. Neurosci.* **31**, 69–89 (2008).
16. J. O'Keefe, J. Dostrovsky, The hippocampus as a spatial map. Preliminary evidence from unit activity in the freely-moving rat. *Brain Res.* **34**, 171–175 (1971).
17. D. C. Rowland, Y. Roudi, M.-B. Moser, E. I. Moser, Ten years of grid cells. *Annu. Rev. Neurosci.* **39**, 19–40 (2016).
18. M.-B. Moser, D. C. Rowland, E. I. Moser, Place cells, grid cells, and memory. *Cold Spring Harb. Perspect. Biol.* **7**, a021808 (2015).
19. J. Jacobs, C. T. Weidemann, J. F. Miller, A. Solway, J. F. Burke, X.-X. Wei, N. Suthana, M. R. Sperling, A. D. Sharan, I. Fried, M. J. Kahana, Direct recordings of grid-like neuronal activity in human spatial navigation. *Nat. Neurosci.* **16**, 1188–1190 (2013).
20. E. A. Maguire, R. Nannery, H. J. Spiers, Navigation around London by a taxi driver with bilateral hippocampal lesions. *Brain* **129**, 2894–2907 (2006).
21. L. R. Squire, The legacy of patient H.M. for neuroscience. *Neuron* **61**, 6–9 (2009).
22. C. F. Doeller, C. Barry, N. Burgess, Evidence for grid cells in a human memory network. *Nature* **463**, 657–661 (2010).
23. L. Kunz, T. N. Schröder, H. Lee, C. Montag, B. Lachmann, R. Sariyska, M. Reuter, R. Stirnberg, T. Stöcker, P. C. Messing-Floeter, J. Fell, C. F. Doeller, N. Axmacher, Reduced grid-cell-like representations in adults at genetic risk for Alzheimer's disease. *Science* **350**, 430–433 (2015).
24. A. O. Constantinescu, J. X. O'Reilly, T. E. J. Behrens, Organizing conceptual knowledge in humans with a grid-like code. *Science* **352**, 1464–1468 (2016).
25. M. Stangl, J. Achtzehn, K. Huber, C. Dietrich, C. Tempelmann, T. Wolbers, Compromised grid-cell-like representations in old age as a key mechanism to explain age-related navigational deficits. *Curr. Biol.* **28**, 1108–1115.e6 (2018).
26. F. C. Hummel, L. G. Cohen, Non-invasive brain stimulation: A new strategy to improve neurorehabilitation after stroke? *Lancet Neurol.* **5**, 708–712 (2006).
27. T. Wagner, F. Fregni, S. Fecteau, A. Grodzinsky, M. Zahn, A. Pascual-Leone, Transcranial direct current stimulation: A computer-based human model study. *Neuroimage* **35**, 1113–1124 (2007).
28. S. Lee, C. Lee, J. Park, C.-H. Im, Individually customized transcranial temporal interference stimulation for focused modulation of deep brain structures: A simulation study with different head models. *Sci. Rep.* **10**, 11730 (2020).
29. N. A. Suthana, Z. Haneef, J. Stern, R. Mukamel, E. Behnke, B. Knowlton, I. Fried, Memory enhancement and deep-brain stimulation of the entorhinal area. *N. Engl. J. Med.* **366**, 502–510 (2012).
30. J. Jacobs, J. Miller, S. A. Lee, T. Coffey, A. J. Watrous, M. R. Sperling, A. Sharan, G. Worrell, B. Berry, B. Lega, B. C. Jobst, K. Davis, R. E. Gross, S. A. Sheth, Y. Ezzyat, S. R. Das, J. Stein, R. Gorniak, M. J. Kahana, D. S. Rizzuto, Direct electrical stimulation of the human entorhinal region and hippocampus impairs memory. *Neuron* **92**, 983–990 (2016).
31. A. Goyal, J. Miller, A. J. Watrous, S. A. Lee, T. Coffey, M. R. Sperling, A. Sharan, G. Worrell, B. Berry, B. Lega, B. C. Jobst, K. A. Davis, C. Inman, S. A. Sheth, P. A. Wanda, Y. Ezzyat, S. R. Das, J. Stein, R. Gorniak, J. Jacobs, Electrical stimulation in hippocampus and entorhinal cortex impairs spatial and temporal memory. *J. Neurosci.* **38**, 4471–4481 (2018).
32. N. Grossman, D. Bono, N. Dedic, S. B. Kodandaramaiah, A. Rudenko, H.-J. Suk, A. M. Cassara, E. Neufeld, N. Kuster, L.-H. Tsai, A. Pascual-Leone, E. S. Boyden, Noninvasive deep brain stimulation via temporally interfering electric fields. *Cell* **169**, 1029–1041.e16 (2017).
33. B. Hutcheon, Y. Yarom, Resonance, oscillation and the intrinsic frequency preferences of neurons. *Trends Neurosci.* **23**, 216–222 (2000).
34. J. Gomez-Tames, A. Asai, A. Hirata, Multiscale computational model reveals nerve response in a mouse model for temporal interference brain stimulation. *Front. Neurosci.* **15**, 684465 (2021).
35. M. J. Wessel, E. Beanato, T. Popa, F. Windel, P. Vassiliadis, P. Menoud, V. Beliaeva, I. R. Violante, H. Abderrahmane, P. Dzialecka, C.-H. Park, P. Maceira-Elvira, T. Morishita, A. M. Cassara, M. Steiner, N. Grossman, E. Neufeld, F. C. Hummel, Noninvasive theta-burst stimulation of the human striatum enhances striatal activity and motor skill learning. *Nat. Neurosci.* **26**, 2005–2016 (2023).
36. P. Vassiliadis, E. Beanato, T. Popa, F. Windel, T. Morishita, E. Neufeld, J. Duque, G. Derosiere, M. J. Wessel, F. C. Hummel, Non-invasive stimulation of the human striatum disrupts reinforcement learning of motor skills. *Nat. Hum. Behav.* **8**, 1–18 (2024).
37. I. R. Violante, K. Alania, A. M. Cassarà, E. Neufeld, E. Acerbo, R. Carron, A. Williamson, D. L. Kurtin, E. Rhodes, A. Hampshire, N. Kuster, E. S. Boyden, A. Pascual-Leone, N. Grossman, Non-invasive temporal interference electrical stimulation of the human hippocampus. *Nat. Neurosci.* **26**, 1994–2004 (2023).
38. T. Popa, E. Beanato, M. J. Wessel, P. Menoud, F. Windel, P. Vassiliadis, I. R. Violante, K. Alania, P. Dzialecka, N. Grossman, E. Neufeld, F. C. Hummel, Effects of hippocampal noninvasive theta-burst stimulation on consolidation of associative memory in healthy older adults. *Neuroscience* **11**, 554933 (2023).
39. N. Grossman, Modulation without surgical intervention. *Science* **361**, 461–462 (2018).

40. E. Arulchelvan, S. Vanneste, Promising neurostimulation routes for targeting the hippocampus to improve episodic memory: A review. *Brain Res.* **1815**, 148457 (2023).
41. T. Hartley, C. Lever, N. Burgess, J. O'Keefe, Space in the brain: How the hippocampal formation supports spatial cognition. *Philos. Trans. R. Soc. Lond. B Biol. Sci.* **369**, 20120510 (2014).
42. Y. Wang, S. Romani, B. Lustig, A. Leonardo, E. Pastalkova, Theta sequences are essential for internally generated hippocampal firing fields. *Nat. Neurosci.* **18**, 282–288 (2015).
43. V. D. Bohbot, M. S. Copara, J. Gotman, A. D. Ekstrom, Low-frequency theta oscillations in the human hippocampus during real-world and virtual navigation. *Nat. Commun.* **8**, 14415 (2017).
44. J. Miller, A. J. Watrous, M. Tsitsiklis, S. A. Lee, S. A. Sheth, C. A. Schevon, E. H. Smith, M. R. Sperling, A. Sharan, A. A. Asadi-Pooya, G. A. Worrell, S. Meisenhelter, C. S. Inman, K. A. Davis, B. Lega, P. A. Wanda, S. R. Das, J. M. Stein, R. Gorniak, J. Jacobs, Lateralized hippocampal oscillations underlie distinct aspects of human spatial memory and navigation. *Nat. Commun.* **9**, 2423 (2018).
45. E. A. Solomon, B. C. Lega, M. R. Sperling, M. J. Kahana, Hippocampal theta codes for distances in semantic and temporal spaces. *Proc. Natl. Acad. Sci. U.S.A.* **116**, 24343–24352 (2019).
46. A. D. Ekstrom, J. B. Caplan, E. Ho, K. Shattuck, I. Fried, M. J. Kahana, Human hippocampal theta activity during virtual navigation. *Hippocampus* **15**, 881–889 (2005).
47. S. Maidenbaum, J. Miller, J. M. Stein, J. Jacobs, Grid-like hexadirectional modulation of human entorhinal theta oscillations. *Proc. Natl. Acad. Sci. U.S.A.* **115**, 10798–10803 (2018).
48. J. Larson, G. Lynch, Induction of synaptic potentiation in hippocampus by patterned stimulation involves two events. *Science* **232**, 985–988 (1986).
49. M. R. Goldsworthy, A.-M. Vallence, N. A. Hodyl, J. G. Semmler, J. B. Pitcher, M. C. Ridding, Probing changes in corticospinal excitability following theta burst stimulation of the human primary motor cortex. *Clin. Neurophysiol.* **127**, 740–747 (2016).
50. A. Suppa, Y.-Z. Huang, K. Funke, M. C. Ridding, B. Cheeran, V. Di Lazzaro, U. Ziemann, J. C. Rothwell, Ten years of theta burst stimulation in humans: Established knowledge, unknowns and prospects. *Brain Stimul.* **9**, 323–335 (2016).
51. P. W. Brownjohn, J. N. J. Reynolds, N. Matheson, J. Fox, J. B. H. Shemmell, The effects of individualized theta burst stimulation on the excitability of the human motor system. *Brain Stimul.* **7**, 260–268 (2014).
52. Y.-Z. Huang, M. J. Edwards, E. Rounis, K. P. Bhatia, J. C. Rothwell, Theta burst stimulation of the human motor cortex. *Neuron* **45**, 201–206 (2005).
53. H.-J. Moon, B. Gauthier, H.-D. Park, N. Faivre, O. Blanke, Sense of self impacts spatial navigation and hexadirectional coding in human entorhinal cortex. *Commun. Biol.* **5**, 406 (2022).
54. S. Kühn, J. Gallinat, Segregating cognitive functions within hippocampal formation: A quantitative meta-analysis on spatial navigation and episodic memory. *Hum. Brain Mapp.* **35**, 1129–1142 (2014).
55. A. Ezzati, M. J. Katz, A. R. Zammit, M. L. Lipton, M. E. Zimmerman, M. J. Sliwinski, R. B. Lipton, Differential association of left and right hippocampal volumes with verbal episodic and spatial memory in older adults. *Neuropsychologia* **93**, 380–385 (2016).
56. E. A. Maguire, R. S. Frackowiak, C. D. Frith, Recalling routes around london: Activation of the right hippocampus in taxi drivers. *J. Neurosci.* **17**, 7103–7110 (1997).
57. M. Boccia, F. Nemmi, C. Guariglia, Neuropsychology of environmental navigation in humans: Review and meta-analysis of FMRI studies in healthy participants. *Neuropsychol. Rev.* **24**, 236–251 (2014).
58. L. Morales-Quezada, J. Leite, S. Carvalho, L. Castillo-Saavedra, C. Cosmo, F. Fregni, Behavioral effects of transcranial pulsed current stimulation (tPCS): Speed-accuracy tradeoff in attention switching task. *Neurosci. Res.* **109**, 48–53 (2016).
59. P. Maceira-Elvira, J. E. Timmermann, T. Popa, A.-C. Schmid, J. W. Krakauer, T. Morishita, M. J. Wessel, F. C. Hummel, Dissecting motor skill acquisition: Spatial coordinates take precedence. *Sci. Adv.* **8**, eabo3505 (2022).
60. H. M. Blumen, Y. Gazes, C. Habeck, A. Kumar, J. Steffener, B. C. Rakitin, Y. Stern, Neural networks associated with the speed-accuracy tradeoff: Evidence from the response signal method. *Behav. Brain Res.* **224**, 397–402 (2011).
61. I. Basu, A. Yousefi, B. Crocker, R. Zelmann, A. C. Paulk, N. Peled, K. K. Ellard, D. S. Weisholtz, G. R. Cosgrove, T. Deckersbach, U. T. Eden, E. N. Eskandar, D. D. Dougherty, S. S. Cash, A. S. Widge, Closed-loop enhancement and neural decoding of cognitive control in humans. *Nat. Biomed. Eng.* **7**, 576–588 (2023).
62. L. M. Giocomo, M.-B. Moser, E. I. Moser, Computational models of grid cells. *Neuron* **71**, 589–603 (2011).
63. R. J. Gardner, E. Hermansen, M. Pachitariu, Y. Burak, N. A. Baas, B. A. Dunn, M.-B. Moser, E. I. Moser, Toroidal topology of population activity in grid cells. *Nature* **602**, 123–128 (2022).
64. T. Stensola, H. Stensola, M.-B. Moser, E. I. Moser, Shearing-induced asymmetry in entorhinal grid cells. *Nature* **518**, 207–212 (2015).
65. A. Bierbrauer, L. Kunz, C. A. Gomes, M. Luhmann, L. Deuker, S. Getzmann, E. Wascher, P. D. Gajewski, J. G. Hengstler, M. Fernandez-Alvarez, M. Atienza, D. M. Cammisuli, F. Bonatti, C. Pruneti, A. Percesepe, Y. Bellaali, B. Hanseeuw, B. A. Strange, J. L. Cantero, N. Axmacher, Unmasking selective path integration deficits in Alzheimer's disease risk carriers. *Sci. Adv.* **6**, eaba1394 (2020).
66. L. Merken, M. Davare, P. Janssen, M. C. Romero, Behavioral effects of continuous theta-burst stimulation in macaque parietal cortex. *Sci. Rep.* **11**, 4511 (2021).
67. C.-T. Li, Y.-Z. Huang, Y.-M. Bai, S.-J. Tsai, T.-P. Su, C.-M. Cheng, Critical role of glutamatergic and GABAergic neurotransmission in the central mechanisms of theta-burst stimulation. *Hum. Brain Mapp.* **40**, 2001–2009 (2019).
68. T. Hartley, E. A. Maguire, H. J. Spiers, N. Burgess, The well-worn route and the path less traveled: Distinct neural bases of route following and wayfinding in humans. *Neuron* **37**, 877–888 (2003).
69. T. Ohnishi, H. Matsuda, M. Hirakata, Y. Ugawa, Navigation ability dependent neural activation in the human brain: An fMRI study. *Neurosci. Res.* **55**, 361–369 (2006).
70. T. I. Brown, V. A. Carr, K. F. LaRocque, S. E. Favila, A. M. Gordon, B. Bowles, J. N. Bailenson, A. D. Wagner, Prospective representation of navigational goals in the human hippocampus. *Science* **352**, 1323–1326 (2016).
71. H. J. Spiers, E. A. Maguire, Thoughts, behaviour, and brain dynamics during navigation in the real world. *Neuroimage* **31**, 1826–1840 (2006).
72. H. J. Spiers, E. A. Maguire, The dynamic nature of cognition during wayfinding. *J. Environ. Psychol.* **28**, 232–249 (2008).
73. L. F. Cobar, L. Yuan, A. Tashiro, Place cells and long-term potentiation in the hippocampus. *Neurobiol. Learn. Mem.* **138**, 206–214 (2017).
74. J. J. Moore, J. D. Cushman, L. Acharya, B. Popeney, M. R. Mehta, Linking hippocampal multiplexed tuning, Hebbian plasticity and navigation. *Nature* **599**, 442–448 (2021).
75. G. Dragoi, K. D. Harris, G. Buzsáki, Place representation within hippocampal networks is modified by long-term potentiation. *Neuron* **39**, 843–853 (2003).
76. C. Kentros, E. Hargreaves, R. D. Hawkins, E. R. Kandel, M. Shapiro, R. V. Muller, Abolition of long-term stability of new hippocampal place cell maps by NMDA receptor blockade. *Science* **280**, 2121–2126 (1998).
77. H. A. Fritch, D. S. Spets, S. D. Slotnick, Functional connectivity with the anterior and posterior hippocampus during spatial memory. *Hippocampus* **31**, 658–668 (2021).
78. J. H. Siegle, M. A. Wilson, Enhancement of encoding and retrieval functions through theta phase-specific manipulation of hippocampus. *eLife* **3**, e03061 (2014).
79. J. von Conta, F. H. Kasten, B. Ćurčić-Blake, A. Aleman, A. Thielscher, C. S. Herrmann, Interindividual variability of electric fields during transcranial temporal interference stimulation (tTIS). *Sci. Rep.* **11**, 20357 (2021).
80. Q. Xiao, Z. Zhong, X. Lai, H. Qin, A multiple modulation synthesis method with high spatial resolution for noninvasive neurostimulation. *PLOS ONE* **14**, e0218293 (2019).
81. J. Cao, P. Grover, STIMULUS: Noninvasive dynamic patterns of neurostimulation using spatio-temporal interference. *I.E.E.E. Trans. Biomed. Eng.* **67**, 726–737 (2019).
82. Y. Huang, A. Datta, L. C. Parra, Optimization of interferential stimulation of the human brain with electrode arrays. *J. Neural Eng.* **17**, 036023 (2020).
83. S. Lee, J. Park, D. S. Choi, C. Lee, C.-H. Im, Multipair transcranial temporal interference stimulation for improved focalized stimulation of deep brain regions: A simulation study. *Comput. Biol. Med.* **143**, 105337 (2022).
84. X. Song, X. Zhao, X. Li, S. Liu, D. Ming, Multi-channel transcranial temporally interfering stimulation (tTIS): Application to living mice brain. *J. Neural Eng.* **18**, 036003 (2021).
85. P. Vassiliadis, E. Stiennon, F. Windel, M. J. Wessel, E. Beanato, F. C. Hummel, Safety, tolerability and blinding efficiency of non-invasive deep transcranial temporal interference stimulation: First experience from more than 250 sessions. *J. Neural Eng.* **21**, 024001 (2024).
86. G. Coughlan, J. Laczó, J. Hort, A.-M. Minihane, M. Hornberger, Spatial navigation deficits — Overlooked cognitive marker for preclinical Alzheimer disease? *Nat. Rev. Neurol.* **14**, 496–506 (2018).
87. J. Laczó, M. Parizkova, S. D. Moffat, Spatial navigation, aging and Alzheimer's disease. *Aging* **10**, 3050–3051 (2018).
88. A. Antal, I. Alekseichuk, M. Bikson, J. Brockmöller, A. R. Brunoni, R. Chen, L. G. Cohen, G. Dowthwaite, J. Ellrich, A. Flöel, F. Fregni, M. S. George, R. Hamilton, J. Haueisen, C. S. Herrmann, F. C. Hummel, J. P. Lefaucheur, D. Liebetanz, C. K. Loo, C. D. McCaig, C. Miniussi, P. C. Miranda, V. Moliadze, M. A. Nitsche, R. Nowak, F. Padberg, A. Pascual-Leone, W. Poppendieck, A. Priori, S. Rossi, P. M. Rossini, J. Rothwell, M. A. Rueger, G. Ruffini, K. Schellhorn, H. R. Siebner, Y. Ugawa, A. Wexler, U. Ziemann, M. Hallett, W. Paulus, Low intensity transcranial electric stimulation: Safety, ethical, legal regulatory and application guidelines. *Clin. Neurophysiol.* **128**, 1774–1809 (2017).
89. M. Seeck, L. Koessler, T. Bast, F. Leijten, C. Michel, C. Baumgartner, B. He, S. Beniczky, The standardized EEG electrode array of the IFCN. *Clin. Neurophysiol.* **128**, 2070–2077 (2017).

90. P. Kunz, A. Antal, M. Hewitt, A. Neef, A. Opitz, W. Paulus, 5 kHz transcranial alternating current stimulation: Lack of cortical excitability changes when grouped in a theta burst pattern. *Front. Hum. Neurosci.* **10**, 683 (2016).
91. J. Larson, E. Munkácsy, Theta-burst LTP. *Brain Res.* **1621**, 38–50 (2015).
92. R. S. Desikan, F. Ségonne, B. Fischl, B. T. Quinn, B. C. Dickerson, D. Blacker, R. L. Buckner, A. M. Dale, R. P. Maguire, B. T. Hyman, M. S. Albert, R. J. Killiany, An automated labeling system for subdividing the human cerebral cortex on MRI scans into gyral based regions of interest. *Neuroimage* **31**, 968–980 (2006).
93. M. Stangl, J. Shine, T. Wolbers, The GridCAT: A toolbox for automated analysis of human grid cell codes in fMRI. *Front. Neuroinform.* **11**, 47 (2017).
94. J. Krogh, I. Bergmann, P. K. Jensen, Retroperitoneal varicose veins simulating lymph nodes. *Urol. Int.* **44**, 319–320 (1989).
95. D. Bates, M. Mächler, B. Bolker, S. Walker, Fitting linear mixed-effects models using lme4. *J. Stat. Softw.* **67**, 1–48 (2014).
96. S. G. Luke, Evaluating significance in linear mixed-effects models in R. *Behav. Res. Methods* **49**, 1494–1502 (2017).
97. R. Lenth, M. R. Lenth, Least-squares means: The R package lsmeans. *Am. Stat.* **34**, 216–221 (2018).
98. M. S. Ben-Shachar, D. Lüdecke, D. Makowski, Effectsize: Estimation of effect size indices and standardized parameters. *J. Open Source Softw.* **5**, 2815 (2020).
99. W. R. Revelle, *psych: Procedures for Personality and Psychological Research* (Northwestern Univ., 2017).
100. T. P. Tavares, "Medial prefrontal cortex (MedPFC)" in *Encyclopedia of Personality and Individual Differences*, V. Zeigler-Hill, T. K. Shackelford, Eds. (Springer International Publishing, 2020), pp. 2827–2830.
101. M. C. Klein-Flügge, A. Bongioanni, M. F. S. Rushworth, Medial and orbital frontal cortex in decision-making and flexible behavior. *Neuron* **110**, 2743–2770 (2022).
102. M. V. Chafee, S. R. Heilbronner, Prefrontal cortex. *Curr. Biol.* **32**, R346–R351 (2022).
103. D. R. Euston, A. J. Gruber, B. L. McNaughton, The role of medial prefrontal cortex in memory and decision making. *Neuron* **76**, 1057–1070 (2012).

Acknowledgments: We acknowledge access to the MRI and Neuromodulation facilities of the Human Neuroscience Platform of the Fondation Campus Biotech Geneva. We thank M. Durand-Ruel and T. Morishita for assistance in randomization and R. Martuzzi, L. Mattera, and O. Reynaud for support in fMRI data acquisition. **Funding:** This work was supported by the Swiss National Science Foundation (SNSF, 320030L_197899, NiBS-iCog) to F.C.H.; the Defitech Foundation (Morges, CH) to F.C.H.; the Bertarelli Foundation - Catalyst program (Gstaad, CH) to F.C.H., M.J.W., T.P., and E.N.; the Wyss Center for Bio and Neuroengineering - AVANCER to F.C.H. and the Lighthouse Partnership for AI-guided Neuromodulation to F.C.H. and O.B.; the Swiss NSF (no. 320030_188798) to O.B.; the Empiris Foundation to O.B.; the Bertarelli Foundation to O.B.; the Fund for Research training in Industry and Agriculture (FRIA/FNRS; FC29690) and Wallonie-Bruxelles International to P.V.; and the ERA-NET NEURON (The DiSCoVer project) to F.C.H; the Korea Institute of Science and Technology (KIST) Institutional Program (2E33141) to H.-J.M. The NEURON "Network of European Funding for Neuroscience Research" is established under the organization of the ERA-NET "European Research Area Networks" of the European Commission to F.C.H. National funding is the Swiss National Science Foundation (SNSF) for EPFL. **Author contributions:** Conceptualization: E.B., H.-J.M., F.W., P.V., T.P., M.J.W., E.D.F., E.N., O.B., and F.C.H. Methodology: E.B., H.-J.M., F.W., P.V., T.P., M.J.W., E.D.F., E.N., O.B., and F.C.H. Software: E.B., H.-J.M., M.S., and E.N. Validation: E.B., F.W., P.V., and F.C.H. Formal analysis: E.B. and H.-J.M. Investigation: E.B., H.-J.M., F.W., P.V., M.W., T.P., P.M., E.D.F., and B.G. Resources: M.S. and F.C.H. Data curation: E.B. Writing—original draft: E.B. and H.-J.M. Writing—review and editing: all coauthors. Visualization: E.B. and H.-J.M. Supervision: E.B., E.N., O.B., and F.C.H. Project administration: E.B., M.W., F.C.H., and E.N. Funding acquisition: O.B., F.C.H., M.J.W., and E.N. **Competing interests:** E.N. is cofounder of TI Solutions AG, a company committed to producing hardware and software solutions to support TI research. O.B. is member of the board and shareholder of Mindmaze SA. The remaining authors declare that they have no competing interests. **Data and materials availability:** All data needed to evaluate the conclusions in the paper are present in the paper and/or the Supplementary Materials. All data necessary to generate the results presented in the figures within this manuscript and the Supplementary Materials are available in the Zenodo repository (10.5281/zenodo.12683782).

Submitted 31 January 2024
Accepted 30 September 2024
Published 30 October 2024
10.1126/sciadv.ado4103